Author Manuscript
Author Manuscript
Author Manuscript
Author Manuscript

HHS Public Access
Author manuscript
Clin Chem. Author manuscript; available in PMC 2023 February 04.

Published in final edited form as:
Clin Chem. 2023 February 01; 69(2): 149–159. doi:10.1093/clinchem/hvac191.

In situ Metabolomics of Cortisol-Producing Adenomas

Masanori Murakami[1,2,*], **Na Sun**[3,*], **Fengxia Li**[3,4], **Annette Feuchtinger**[3], **Celso Gomez-Sanchez**[5], **Martin Fassnacht**[6], **Martin Reincke**[1], **Irina Bancos**[7], **Axel Walch**[3], **Matthias Kroiss**[1,6,8,†], **Felix Beuschlein, M.D.**[1,9,†]

[1]Medizinische Klinik und Poliklinik IV, Klinikum der Universität, Ludwig-Maximilians-Universität München, Munich, Germany

[2]Department of Molecular Endocrinology and Metabolism, Graduate School of Medical and Dental Sciences, Tokyo Medical and Dental University, Tokyo, Japan

[3]Research Unit Analytical Pathology, Helmholtz Zentrum München, German Research Center for Environmental Health (GmbH), Neuherberg, Germany

[4]Department of Neuro- and Sensory Physiology, University Medical Center Göttingen, Göttingen, Germany

[5]Division of Endocrinology, G.V. (Sonny) Montgomery VA Medical Center and the University of Mississippi Medical Center, Jackson, Mississippi, USA

[6]Department of Internal Medicine I, Division of Endocrinology and Diabetology, University Hospital Würzburg, University of Würzburg, Würzburg, Germany

[7]Division of Endocrinology, Mayo Clinic, Rochester, Minnesota, USA

[8]Comprehensive Cancer Center Mainfranken, University of Würzburg, Würzburg, Germany

[9]Department of Endocrinology, Diabetology and Clinical Nutrition, University Hospital Zurich (USZ) and University of Zurich (UZH), Zurich, Switzerland

Abstract

Corresponding author and person to whom reprint requests: Prof. Felix Beuschlein, M.D., Klinik für Endokrinologie, Diabetologie und Klinische Ernährung, Universitätsspital Zürich, Raemistrasse 100, CH-8091 Zürich, Switzerland, Phone: +41 44 255 36 25, Fax: +41 44 255 33 30, felix.beuschlein@usz.ch.
*M Murakami and N Sun contributed equally as first authors
†M Kroiss and F Beuschlein contributed equally as senior authors

Author Contributions
M.R., M.F., M.K. and F.B. designed the research. I.B. collected samples and clinical data from patients. M.M., N.S., F.L., A.F., C.G.S., A.W., M.F., M.K. and F.B. performed immunostaining, and MALDI-FT-ICR MSI analysis or performed statistical analysis of results. M.M., N.S., M.K. and F.B. drafted the manuscript, and all authors contributed to writing the manuscript and approved the version to be published.

Authors' Disclosures or Potential Conflicts of Interest
Upon manuscript submission, all authors completed the author disclosure form.

Employment or Leadership: None declared.

Consultant or Advisory Role: None declared.

Stock Ownership: None declared.

Honoraria: None declared.

Expert Testimony: None declared.

Patents: None declared.

Author Manuscript Author Manuscript Author Manuscript Author Manuscript

BACKGROUND: Recent advances in omics techniques have allowed detailed genetic characterization of cortisol-producing adrenal adenoma (CPA). In contrast, the pathophysiology of CPAs has not been elucidated in detail on the level of tumor metabolic alterations.

METHODS: The current study conducted a comprehensive mass spectrometry imaging (MSI) map of CPAs in relation to clinical phenotypes and immunohistochemical profiles of steroidogenic enzymes. The study cohort comprised 46 patients with adrenal tumors including CPAs (n = 35) and non-functional adenomas (n = 11).

RESULTS: Severity of cortisol hypersecretion was significantly correlated with 29 metabolites (adjusted P <0.05). Adrenal androgens derived from the classic androgen pathway were inversely correlated with both cortisol secretion (r_s = −0.41, adjusted P = 0.035) and CYP11B1 expression (r_s = −0.77, adjusted P = 2.00E-08). The extent of cortisol excess and tumor CYP11B1 expression further correlated with serotonin (r_s = 0.48 and 0.62, adjusted P = 0.008 and 2.41E-05). Tumor size was found to be correlated with abundance of 13 fatty acids (adjusted P <0.05) and negatively associated with 9 polyunsaturated fatty acids including phosphatidic acid 38:8 (r_s = −0.56, adjusted P = 0.009).

CONCLUSIONS: MSI reveals novel metabolic links between endocrine function and tumorigenesis, which will further support the understanding of CPA pathophysiology.

Keywords

Cushing syndrome; adrenal adenoma; metabolome; steroidogenic enzyme; cortisol

Introduction

Cortisol-producing adenomas (CPA) are characterized by their ability to secrete cortisol with independence from pituitary ACTH. The degree of systemic hypercortisolism is widely variable, ranging from subtle alterations of the hypothalamic-pituitary-adrenal (HPA) axis in the absence of clinical signs of hypercortisolism to overt Cushing's syndrome. Likewise, the clinical spectrum of hypercortisolism differs depending on the degree of cortisol secretion and target tissue response, ranging from mild metabolic alterations to severe metabolic, cardiovascular and infectious co-morbidities (1–4), which increase mortality (5). However, even hypercortisolism without overt Cushingoid features, in which cortisol excess was diagnosed based on the dexamethasone suppression test, has been demonstrated to have long-term adverse consequences on various clinical parameters (6). Therefore, recent guidelines from the European Society of Endocrinology (ESE) and the European Network for the Study of Adrenal Tumors (ENS@T) have provided diagnostic criteria to grade the degree of hypercortisolism as possible autonomous cortisol secretion (PACS) and autonomous cortisol secretion (ACS), based on the low dose dexamethasone suppression test results (7).

Over the last decades, the pathogenesis of CPAs has been studied at the molecular and genetic level, which has revealed recurrent somatic mutations of the gene encoding the catalytic subunit of protein kinase A (*PRKACA*), α-subunit of the stimulatory G protein (*GNAS*) and β-catenin (*CTNNB1*) (8). Likewise, variable secretion of glucocorticoids, androgens and other steroid hormone precursors has prompted steroid metabolome studies

Author Manuscript Author Manuscript Author Manuscript Author Manuscript

in plasma and urine samples (9–13), which demonstrated associations of steroid signatures with clinical characteristics. Examples include lower levels of 11-deoxycortisol and 11-deoxycorticosterone observed in subclinical hypercortisolism compared to overt Cushing syndrome (12). The metabolic and epigenetic impact of hypercortisolism in CPA has been demonstrated by targeted plasma metabolomics (14) and blood methylome analysis (15), thus reflecting systemic responses to hypercortisolism.

Current advances in matrix-assisted laser desorption/ionization mass spectrometry imaging (MALDI-MSI) have permitted the superimposing of metabolome data on the spatial information from conventional histology. This technique has recently allowed us to refine the functional anatomy of the human adrenal gland (16, 17), has provided novel biomarkers and pathways associated with malignant behavior in adrenocortical carcinoma (18) and has yielded insight into genotype/phenotype correlations of aldosterone-producing adenoma (19), and pheochromocytoma and paraganglioma (20). Based on a similar technique, tissue steroid profiles of optimal cutting temperature compound (OCT)-embedded CPA were investigated and 19 steroids were successfully identified (21). Here, we report the first comprehensive MALDI-MSI study of a set of cortisol-producing adenomas with clinical information in order to gain further insights into their pathogenesis.

Materials and Methods

Patient cohort

A total of 46 adrenal tumors were retrieved from the Mayo Clinic, Rochester, MN, US. Clinical and hormonal data were collected through the ENS@T registry (https://registry.ensat.org/). Patients with Cushing syndrome (CS), autonomous cortisol secretion (ACS), possible autonomous cortisol secretion (PACS), and non-functional adenoma (NFA) were diagnosed according to current guidelines (7) following dexamethasone suppression test. As a result, plasma cortisol concentrations after low dose dexamethasone suppression test (LDDST) in patients with CS, ACS and PACS were higher than in those with NFA (P <0.05, Table 1).

Tissue microarrays, immunohistochemistry, and digital image analysis.

Tissue Microarrays (TMAs) were constructed using the ISENET Galileo CK4500 with core diameters of 1.0mm. Experimental tissues were placed within the array in a specified layout. TMA cores were set within the paraffin array by incubating at 39C for 1 hour. Paraffin-embedded tissue blocks were selected based on selection of representative areas on the basis of hematoxylin and eosin (H&E) stained tissue sections by the experienced pathologists.

A semi-automated rotation microtome (Microm HM 355S, Thermo Fisher Scientific, MA) was used to cut 3-μm tissue microarray sections that were transferred to glass slides for immunohistochemistry (IHC) and H&E staining. IHC staining was performed on a Discovery XT automated stainer (Roche Diagnostics/Ventana Medical Systems, AZ) according to the manufacturer's instructions, employing monoclonal antibodies directed against human cytochrome P450 family 11 subfamily B member 1 (CYP11B1), cytochrome

Author Manuscript Author Manuscript Author Manuscript Author Manuscript

P450 family 11 subfamily B member 2 (CYP11B2), cytochrome P450 family 17 subfamily A member 1 (CYP17A1) (22), hydroxy-delta-5-steroid dehydrogenase, 3 beta- and steroid delta-isomerase 1 (HSD3B1) (23) and polyclonal antibody against hydroxy-delta-5-steroid dehydrogenase, 3 beta- and steroid delta-isomerase 2 (HSD3B2). Slides were incubated with primary antibodies (rat monoclonal anti-hCYP11B1 [1:20], mouse monoclonal anti-hCYP11B2 [1:100], mouse monoclonal anti-17α-hydroxylase [1:500], mouse monoclonal anti-hHSD3B1 [1:500], or rabbit polyclonal anti-hHSD3B2 [1:250] (Abcam, catalog Ab154385, Cambridge, UK), in Dako REAL antibody dilution, Agilent, CA), and detected by the Discovery DAB Map Kit (Roche Diagnostics/Ventana Medical Systems), including incubation with respective secondary antibodies (For CYP11B2, CYP17A1, HSD3B1, HSD3B2: anti-mouse and anti-rabbit, ready-to-use universal secondary antibody, catalog 760-4205, Roche Diagnostics/Ventana Medical Systems; For CYP11B1: anti-rat, ready-to-use universal secondary antibody, catalog BA-4000, Vector Laboratories, CA). Appropriate positive and negative controls were included in each staining procedure.

Following H&E staining and IHC, tissue microarray slides were scanned at ×20 objective magnification using a digital Mirax Desk slide scanner (Carl Zeiss Microscopy GmbH, Jena, Germany) prior to import into the image analysis software Definiens Developer XD2 (Definiens AG, Munich, Germany), as described previously (24). Tumor areas were manually annotated, and a rule set, which was described in the previous article (24), was defined to detect and quantify staining intensities from IHC in the annotated tumor area, with operators blinded with regard to corresponding clinical annotations.

Sample preparation and MALDI-MSI

TMA samples were sectioned with a thickness of 3 μm, and water-bath mounted onto indium-tin oxide (ITO)-coated glass slides (Bruker Daltonik GmbH, Bremen, Germany). FFPE sections were incubated for 1 h at 70°C, de-paraffinized in xylene (2 × 8 min), and air-dried. For MALDI-MSI of endogenous metabolites, the matrix solution was 10 mg/ml 9-aminoacridine hydrochloride monohydrate matrix (9-AA) (Sigma-Aldrich Chemie GmbH, Munich, Germany) in water/methanol 30:70 (v/v). 9-AA was chosen as a matrix since it is known to exhibit very few matrix-derived interferences in the low-mass range and to achieve high sensitivity and high linearity in negative ion mode for a wide range of low molecular-weight metabolites (25–29). The matrix solution was sprayed on the tissue sections using a SunCollect automatic sprayer (SunChrom, Friedrichsdorf, Germany) at room temperature. The matrix application was performed at flow rates of 10, 20, 30 and 40 μL/min, respectively, for the first four layers. The other four layers were performed at 40 μL/min.

Following tissue sample preparation, the MALDI-MSI measurement was performed on a on an Ultraflex III MALDI-TOF/TOF MS equipped with a Smartbeam-II Nd:YAG laser at a frequency of 100 Hz (Bruker Daltonics, Bremen, Germany). The setting for the sampling rate was 2.0 GS/s, and a total of 200 laser shots were used for a measurement position. The MALDI-MSI data were acquired over a mass range of m/z 80–1000. Mass imaging data were acquired in reflector negative ionization mode with 70 μm spatial resolution. The mass spectrometer was calibrated using red phosphorus (Sigma-Aldrich,

Author Manuscript Author Manuscript Author Manuscript Author Manuscript

Taufkirchen, Germany), which was dissolved in acetone and spotted (1 μL) on the same glass slide into an area with matrix. After the MALDI-MSI measurement, the acquired data from the tissue samples underwent spectra processing in FlexImaging v. 4.2 (Bruker Daltonics, Bremen, Germany). Following the MALDI imaging, matrix was removed with 70% ethanol. Tissue sections were stained with H&E and scanned with a digital Mirax Desk slide scanner (Zeiss, Göttingen, Germany). Metabolite annotation was performed using the Human Metabolome Database (HMDB, http://www.hmdb.ca/) (30) and Kyoto Encyclopedia of Genes and Genomes (KEGG) database (http://www.genome.jp/kegg/) (31). Pathway enrichment analysis was applied to identify discriminative features of CPAs, using Metabolite Set Enrichment Analysis with MetaboAnalyst (http://www.metaboanalyst.ca) (32).

Phospholipids were annotated by lipid subclass such as PA, phosphatidic acid; PC, phosphatidylcholine; PE, phosphatidylethanolamine; PI, phosphatidylinositol; PS, phosphatidylserine, followed by “the total acyl chain length: total number of unsaturated bonds” (e.g., PA 32:1). The lyso form was denoted with “lyso”. All the detected phospholipids, with classification of the proportion of unsaturations which classify fatty acids, including 0 double bonds as saturated fatty acids (SFA), one double bonds as monounsaturated fatty acid (MUFA) and more than one double bonds as polyunsaturated fatty acid (PUFA), are shown in Supplemental Table 1.

Bioinformatics and statistical analysis

MS data were normalized to the total ion count. Peak picking was done using mMass software version 5.5.0 (33) as described in detail previously (34). Briefly, smoothing and peak picking was conducted in mMass using the Savitzky-Golay algorithm (0.25 m/z window size, 2 cycles) and a S/N of 1. List of m/z species with respective intensities for ROIs were uploaded to MetaboAnalyst (http://www.metaboanalyst.ca) (35). Heatmap-based clustering was created with MetaboAnalyst and data were exported as figures.

Statistical comparisons between IHC, metabolome, and phenotype were performed with Mann-Whitney U test, Kruskal-Wallis test, or Spearman’s rank correlation test. Spearman’s coefficients are denoted by r_s. Correction for multiple comparisons were calculated with the Benjamini–Hochberg correction and adjusted p-values are shown. All calculations were performed using R 3.4.3.

Results

Demographics and steroidogenic enzyme expression

Clinical characteristics of 46 patients (10 men / 36 women with a median age at surgery of 51 (39 – 60) years) with adrenal tumors are summarized and stratified by the level of autonomous cortisol secretion in Table 1. Following IHC of steroidogenic enzymes, including CYP11B1, CYP11B2, CYP17A1, HSD3B1 and HSD3B2, and assessment of staining intensities (Figure 1A and Supplemental Figure 1), we confirmed a significant association of CYP11B1 expression and the cortisol-secretion phenotype (Figure 1A and B).

Author Manuscript Author Manuscript Author Manuscript Author Manuscript

Metabolome profiles and phenotype correlation

Following MALDI MSI analysis, 603 m/z species over a mass range of 80–1000 *m/z* were detected. Unsupervised hierarchical clustering analysis for cortisol-secretion phenotype discriminated between a low cortisol-producing group (mainly clinically defined as NFA) and high cortisol producing group (mainly including CS, Figure 2A). In addition, correlations between metabolome profiles and LDDST demonstrated significant associations with 96 metabolites. Among those, 29 metabolites were successfully annotated (Supplemental Table 2). A further 67 metabolites could not be annotated because of the lack of an endogenous candidate in the database, and hence were excluded from further analysis. A negative correlation of tissue abundance of steroid-related precursors 3a-hydroxy-5b-pregnane-20-one (*m/z* 353.226) and C19H28O2(*m/z* 309.186) with cortisol following LDDST was observed (r_s = −0.39 and −0.41, adjusted P = 0.046 and 0.035, respectively, Supplemental Table 2). C19H28O2 reflects the isobaric adrenal androgens derived from the classic androgen pathway (classic adrenal androgens): dehydroepiandrosterone (DHEA), androstanedione and testosterone, which could not be distinguished from each other in the applied technique. In addition, regarding steroid-related metabolites, 3a-hydroxy-5b-pregnane-20-one, C19H28O2 and sulfated metabolites cholesterol sulfate (*m/z* 503.258), and C19H28O5S(*m/z* 405.117) were found to have significant differences in a group-wise comparison between clinical phenotypes (P = 0.007, 0.005, 0.019 and 0.012, respectively, Figure 2B and C). C19H28O5S reflects the classic adrenal androgen sulfates: dehydroepiandrosterone sulfate (DHEAS), epitestosterone sulfate and testosterone sulfate.

We further identified a positive correlation between the level of hypercortisolism (based on LDDST) and metabolites from tryptophan related metabolism, including N-acetylserotonin (*m/z* 253.074), 5-hydroxy-N-formylkynurenine (*m/z* 251.069) and serotonin (*m/z* 213.042) (r_s = 0.60, 0.53 and 0.48, adjusted P = 0.001, 0.004, and 0.008, respectively, Supplemental Table 2), with highly significant group-wise differences (P = 8.70E-05, 2.80E-04 and 0.007, respectively, Figure 2D and E). One of the metabolites from tryptophan metabolism, 4,6-dihydroxyquinoline (*m/z* 142.03) also showed differential distribution with cortisol-secretion phenotype (P = 0.043, Figure 2D). Notably, thymidine (*m/z* 263.063) from pyrimidine metabolism, metanephrine (*m/z* 196.098) from tyrosine metabolism and ubiquinone-1 (*m/z* 285.09) from ubiquinone biosynthesis were among the metabolites which showed positive correlation with cortisol following LDDST (r_s = 0.65, 0.50 and 0.53, adjusted P = 4.38E-04, 0.006 and 0.004, respectively, Supplemental Table 2).

Correlation of tumor metabolite content and steroidogenic enzyme expression.

Comparison between metabolites and staining intensity of CYP11B1 revealed significant correlation of 254 metabolites (adjusted P <0.05) of which 65 metabolites were annotated (Supplemental Table 3). As expected, steroid-related metabolites (including cholesterol sulfate, 3a-hydroxy-5b-pregnane-20-one, C19H28O2 and C19H28O5S) which were correlated with the cortisol-secretion phenotype were also inversely correlated with staining intensity of CYP11B1 (r_s = −0.69, −0.77, −0.77 and −0.75, adjusted P = 8.64E-07, 1.62E-08, 2.00E-08 and 5.60E-08, respectively, Supplemental Table 3 and Figure 3). In addition, 3beta-hydroxypregn-5-en-20-one sulfate (*m/z* 433.144), 18-hydroxycortisol (*m/z* 415.150) and 17-beta-estradiol-3,17-beta-sulfate (*m/z* 431.081) were also inversely

Author Manuscript Author Manuscript Author Manuscript Author Manuscript

correlated with staining intensity of CYP11B1 (r_s = −0.72, −0.52 and −0.44, adjusted P = 2.17E-07, 7.50E-04 and 0.007, respectively, Supplemental Table 3 and Figure 3). Positive correlation between metabolites from tryptophan metabolism including 5-hydroxy-N-formylkynurenine, serotonin, N-acetylserotonin and 4,6-dihydroxyquinoline, were also observed (r_s = 0.78, 0.62, 0.61 and 0.56, adjusted P = 1.24E-08, 2.41E-05, 4.38E-05 and 2.05E-04, respectively, Supplemental Table 3 and Figure 3).

Among lipids, specific phospholipids and lysophospholipids were correlated with staining intensity of CYP11B1. For example, lysoPA 22:0 (*m/z* 531.288), PA 31:2 (*m/z* 667.375), lysoPA 21:0 (*m/z* 517.273), PA 32:5 (*m/z* 673.361) and PA 34:1 (*m/z* 711.436) showed an inverse correlation with staining intensity of CYP11B1 (r_s = −0.79, −0.77, −0.77, −0.67 and −0.42, adjusted P = 8.89E-09, 1.54E-08, 1.62E-08, 3.43E-06 and 0.010, respectively, Supplemental Table 3 and Figure 3). In contrast, lysoPC 18:4 (*m/z* 496.281), lysoPC P-16:0 (*m/z* 514.309) and lysoPC 19:1 (*m/z* 572.313) were positively correlated with staining intensity of CYP11B1 (r_s = 0.62, 0.36 and 0.36, adjusted P = 2.99E-05, 0.034 and 0.035, respectively, Supplemental Table 3 and Figure 3).

Correlation of tumor metabolite content and tumor size.

Comparison between metabolites and tumor size revealed significant correlations of 50 metabolites (adjusted P <0.05) with 17 metabolites being annotated. Notably, 13 metabolites were annotated as inversely correlation phospholipids (Figure 4) including PS 28:0 (*m/z* 714.409), PA 38:8 (*m/z* 697.423) and PA 35:5 (*m/z* 715.408, r_s = −0.60, −0.56 and −0.51, adjusted P = 0.007, 0.009 and 0.014, respectively, Figure 4A and B). Notably, there were some exceptions among samples, which did not follow the general trend observed in relation to size. Nine out of 13 metabolites correlated with tumor size were phospholipids with poly-unsaturated fatty acids (PUFAs), which accounted for 45.0% (9/20) of all the detected PUFAs in our analysis. In contrast, only 3 SFAs and 1 MUFA were correlated with tumor size, which accounted for 15.0% (3/20) of detected SFAs and 14.3% (1/7) of detected MUFAs, respectively. Other than phospholipids, only 4 metabolites were significantly correlated with tumor size (Supplemental Table 4). These include C21H32O4 (*m/z* 385.178), possibly annotated as 17alpha,21-dihydroxypregnenolone or 3a,21-dihydroxy-5b-pregnane-11,20-dione (r_s = 0.47, adjusted P = 0.025 Supplemental Table 4).

Discussion

This is the first study to examine the intra-tumoral metabolome of a spectrum of adrenocortical tumors with or without glucocorticoid excess by MALDI-mass spectrometry imaging. Based on the current untargeted metabolomic profiles, we provide insights into specific metabolic changes related to cortisol secretion, steroidogenic enzyme expression and tumor size.

A previous study had demonstrated higher CYP11B1 expression in CPA (36), which is supported by our digital image data confirming intensity of CYP11B1 associated with group wise differences inthe cortisol-secretion phenotype. Consistent with the role of 11 beta hydroxylase as a rate limiting step of cortisol production, a gradual increase in the expression of this enzyme with the level of cortisol autonomy (as reflected by the

Author Manuscript Author Manuscript Author Manuscript Author Manuscript

cortisol level upon LDDST) was evident. In addition to this expected correlation between clinical and tissue-based annotations, we found that metabolome clustering separates tumors producing less cortisol, with a clinically mild phenotype, from tumors producing more cortisol, with a clinically more severe phenotype.

Among the intra-tumor metabolites that separated well between the clinically defined entities were classic adrenal androgens and their sulfated forms. The latter can be accessed particularly easily by the applied method when formalin fixed paraffin embedded tissue is used. In fact, certain sulfated steroids have been demonstrated to be prognostic markers in adrenocortical carcinoma (18). Low systemic concentrations of classic adrenal androgens are a well-appreciated feature of patients with adrenal Cushingś syndrome that result from suppressed HPA activity, with consecutively lower production of ACTH dependent adrenal androgens. (9, 10, 12, 13). Notably, a previous study on OCT samples from CPA and adjacent normal adrenals had not been able to show differences in adrenal androgen concentrations in relation to the clinical phenotype (21). In contrast, our analysis including NFA, PACS and ACS reveals differences in classic adrenal androgen production in adrenal adenoma, which might be modulated by ACTH and result in less abundance of classic adrenal androgens in CPAs. In addition, the adrenal gland is capable of synthesizing 11-oxygenated androgens e.g. through conversion of androstenedione to 11beta-hydroxyandrostendione, a step catalyzed by CYP11B1 (37). In accordance with this, urinary 11beta-hydroxyandrostendione output was associated with CYP11B1 expression in tissues of aldosterone producing adrenocortical adenomas (38). It is conceivable that the inverse correlation between classic adrenal androgens and CYP11B1 expression may be associated with increases in 11-oxygenated androgens which we were unable to detect in tissue samples, possibly due to technical limitations.

In addition to classic adrenal androgens, cholesterol sulfate was found to be less abundant in tumors with higher cortisol-secretion ability. A previous study had suggested tumor heterogeneity in CPA with morphologically compact cells being the hormonally active cell population and clear cells being considered hormonally quiescent based on the expression of steroidogenic enzymes(39). Here, we add support to this notion by showing cholesterol - represented by its sulfate in our experimental setting - to negatively correlate with glucocorticoid secretion, which goes beyond morphological characteristics. Because compact cells have lower content in lipid droplets and hence less cholesterol and cholesterol esters, our finding of low abundance of the detectable cholesterol metabolite cholesterol sulfate is well in line with activation of cortisol secretion. Interestingly, metabolites related to tryptophan metabolism were positively correlated with both cortisol-secretion phenotype and CYP11B1 expression in our study. In the human adrenal cortex, serotonin, released by mast cells, has been demonstrated to stimulate corticoid secretion through activation of type 4 serotonin receptors (5-HT_4R). Accordingly, a recent study had demonstrated overexpression of tryptophan hydroxylase and serotonin receptors in cortisol-producing tumors (44). Tryptophan hydroxylase catalyzes tryptophan 5-hydroxylation leading to 5-hydroxytryptophan which further undergoes decarboxylation to serotonin. The serotonin metabolites 5-hydroxy-N-formylkynurenine, acetylserotonin and 4,6-dihydroxyquinoline were found to be associated with the cortisol-secretion phenotype, supporting the pathophysiological relevance of serotonin signaling in CPAs.

Author Manuscript Author Manuscript Author Manuscript Author Manuscript

Specific lipid metabolites were correlated with CYP11B1 expression and tumor size, respectively. Beyond the function of phospholipids in cellular membranes, lipids are an integral part of signal transduction in numerous cellular processes (45). Abundance of lysoPA was inversely correlated and that of lysoPC positively correlated with CYP11B1 expression. LysoPA is produced from lysoPC by lysophospholipase D (LPD) such as autotaxin or from phosphatidic acid by PA selective phospholipases A1 and A2, and signals through G protein coupled receptors. The role of LysoPC and LysoPA in the adrenal cortex has not specifically been investigated although a function in the adrenal medulla has been proposed (46). While from our observation no direct evidence can be drawn for a functional role of lipid signaling within the spectrum of NFA to CPA, it opens an interesting new avenue for further research with the hypothesis that genetic activation of the cAMP-PKA pathway in CPA may outweigh the activation of the PKA pathway by lyso-phospholipids. Our study also revealed lower accumulation of 13 phospholipids including 9 PUFAs in larger tumors. It is known that *de novo* lipogenesis of saturated fatty acids and monounsaturated fatty acids in neoplastic cells contributes to the maintenance of stable cell membranes and protects against lipid peroxidation (47). On the other hand, adrenal cortical cells require PUFAs to maintain steroidogenesis, with cholesterol-esters in lipid droplets containing predominantly long-chain PUFAs (48). We speculate that lower accumulation of PUFAs may be indicative of lower cholesterol ester stores caused by PKA activation. Our findings provide new insights into relationship between the quality of lipid (lipoquality) and endocrine tumors.

Our study has some limitations: Firstly, this study relied on FFPE tissue samples that - through their specific preparation – deplete highly lipophilic metabolites while hydrophilic metabolites such as lipid sulfates are comparably enriched. Single m/z species may correspond to several metabolites and their identity cannot be identified with certainty. However, although alternative annotations exist for some m/z s, most are structural variants of the same compound with the possibility of assessing likely presence according to mass accuracy, adduct, or plausibility. Secondly, information about genetic alterations, e.g. of the PKA pathway, was unavailable, rendering a direct comparison between metabolites and genetic status a subject for future studies. On the other hand, the homogeneity of the samples from a single center with availability of clinical information after uniform endocrine workup enabled the unique correlation of MALDI MSI data with clinical features of steroid hormone excess.

The present study is the first to comprehensively assess metabolic profiles of CPAs with regard to cortisol-secretion phenotype. Adrenal androgens and their sulfated metabolites and metabolites from tryptophan metabolism showed correlation with both cortisol-secretion phenotype and expression of CYP11B1. Correlations between lysophospholipids and CYP11B1 expression and the inverse correlation between PUFAs and tumor size provide new evidence supporting the study of these signaling molecules in the future.

Supplementary Material

Refer to Web version on PubMed Central for supplementary material.

Author Manuscript Author Manuscript Author Manuscript Author Manuscript

Acknowledgement

The authors would like to thank Ulrike Buchholz, Claudia-Mareike Pflüger, Andreas Voss, Jana Drechsler, Brigitte Mauracher, Petra Rank, Christina Brugger and Kerstin Schaefer for excellent technical assistance.

Research Funding:

This study was supported by the German Research Foundation (DFG) project number 314061271 (CRC/TRR 205) to M.K., F.B., M. R., M.F. and A.K.W and by the Clinical Research Priority Program of the University of Zurich for the CRPP HYRENE to F.B.

M.M. was supported by the Japan Heart Foundation/Bayer Yakuhin Research Grant Abroad and a postdoctoral fellowship of the Uehara Memorial Foundation. This research was partly supported by the National Institute of Diabetes and Digestive and Kidney Diseases (NIDDK) of the National Institutes of Health (NIH) USA under award K23DK121888 (to I.B.) and award R03DK132121 (to I.B). The views expressed are those of the author(s) and not necessarily those of the National Institutes of Health USA.

Role of Sponsor:

The funding organizations played no role in the design of study, choice of enrolled patients, review and interpretation ofdata, preparation of manuscript, or final approval of manuscript.

Nonstandard abbreviations:

CPA	cortisol-producing adenoma
ACTH	adrenocorticotropic hormone
HPA	hypothalamic-pituitary-adrenal
ESE	European Society of Endocrinology
ENS@T	European Network for the Study of Adrenal Tumors
PACS	possible autonomous cortisol secretion
ACS	autonomous cortisol secretion
MALDI-MSI	matrix-assisted laser desorption/ionization mass spectrometry imaging
OCT	optimal cutting temperature compound
NFA	non-functional adenoma
LDDST	low dose dexamethasone suppression test
TMA	tissue microarray
FFPE	formalin-fixed, paraffin-embedded
HMDB	Human Metabolome Database
KEGG	Kyoto Encyclopedia of Genes and Genomes
PA	phosphatidic acid
PC	phosphatidylcholine

Author Manuscript Author Manuscript Author Manuscript Author Manuscript

PE	phosphatidylethanolamine
PI	phosphatidylinositol
PS	phosphatidylserine
SFA	saturated fatty acid
MUFA	monounsaturated fatty acid
PUFA	polyunsaturated fatty acid
ROI	region of interest
DHEA	dehydroepiandrosterone
DHEAS	dehydroepiandrosterone sulfate
PKA	protein kinase A

References

1. Di Dalmazi G, Vicennati V, Rinaldi E, Morselli-Labate AM, Giampalma E, Mosconi C, et al. Progressively increased patterns of subclinical cortisol hypersecretion in adrenal incidentalomas differently predict major metabolic and cardiovascular outcomes: A large cross-sectional study. Eur J Endocrinol 2012;166:669–77. [PubMed: 22267278]
2. Erbil Y, Ademoglu E, Ozbey N, Barbaros U, Yanik BT, Salmaslioglu A, et al. Evaluation of the cardiovascular risk in patients with subclinical cushing syndrome before and after surgery. World J Surg 2006;30:1665–71. [PubMed: 16927063]
3. Orth DN. Cushing's syndrome. N Engl J Med 1995;332:791–803. [PubMed: 7862184]
4. Chiodini I, Guglielmi G, Battista C, Carnevale V, Torlontano M, Cammisa M, et al. Spinal volumetric bone mineral density and vertebral fractures in female patients with adrenal incidentalomas: The effects of subclinical hypercortisolism and gonadal status. J Clin Endocrinol Metab 2004;89:2237–41. [PubMed: 15126547]
5. Graversen D, Vestergaard P, Stochholm K, Gravholt CH, Jorgensen JO. Mortality in cushing's syndrome: A systematic review and meta-analysis. Eur J Intern Med 2012;23:278–82. [PubMed: 22385888]
6. Prete A, Subramanian A, Bancos I, Chortis V, Tsagarakis S, Lang K, et al. Cardiometabolic disease burden and steroid excretion in benign adrenal tumors : A cross-sectional multicenter study. Ann Intern Med 2022;175:325–34. [PubMed: 34978855]
7. Fassnacht M, Arlt W, Bancos I, Dralle H, Newell-Price J, Sahdev A, et al. Management of adrenal incidentalomas: European society of endocrinology clinical practice guideline in collaboration with the european network for the study of adrenal tumors. Eur J Endocrinol 2016;175:G1–G34. [PubMed: 27390021]
8. Vaduva P, Bonnet F, Bertherat J. Molecular basis of primary aldosteronism and adrenal cushing syndrome. J Endocr Soc 2020;4:bvaa075. [PubMed: 32783015]
9. Di Dalmazi G, Fanelli F, Zavatta G, Ricci Bitti S, Mezzullo M, Repaci A, et al. The steroid profile of adrenal incidentalomas: Subtyping subjects with high cardiovascular risk. J Clin Endocrinol Metab 2019;104:5519–28. [PubMed: 31381072]
10. Di Dalmazi G, Fanelli F, Mezzullo M, Casadio E, Rinaldi E, Garelli S, et al. Steroid profiling by lc-ms/ms in nonsecreting and subclinical cortisol-secreting adrenocortical adenomas. J Clin Endocrinol Metab 2015;100:3529–38. [PubMed: 26161451]
11. Eisenhofer G, Masjkur J, Peitzsch M, Di Dalmazi G, Bidlingmaier M, Gruber M, et al. Plasma steroid metabolome profiling for diagnosis and subtyping patients with cushing syndrome. Clin Chem 2018;64:586–96. [PubMed: 29208661]

Author Manuscript Author Manuscript Author Manuscript Author Manuscript

12. Masjkur J, Gruber M, Peitzsch M, Kaden D, Di Dalmazi G, Bidlingmaier M, et al. Plasma steroid profiles in subclinical compared with overt adrenal cushing syndrome. J Clin Endocrinol Metab 2019;104:4331–40. [PubMed: 30977834]
13. Hana V Jr., Jezkova J, Kosak M, Krsek M, Hana V, Hill M. Serum steroid profiling in cushing's syndrome patients. J Steroid Biochem Mol Biol 2019;192:105410. [PubMed: 31201926]
14. Di Dalmazi G, Quinkler M, Deutschbein T, Prehn C, Rayes N, Kroiss M, et al. Cortisol-related metabolic alterations assessed by mass spectrometry assay in patients with cushing's syndrome. Eur J Endocrinol 2017;177:227–37. [PubMed: 28566446]
15. Armignacco R, Jouinot A, Bouys L, Septier A, Lartigue T, Neou M, et al. Identification of glucocorticoid-related molecular signature by whole blood methylome analysis. Eur J Endocrinol 2022;186:297–308. [PubMed: 34914631]
16. Sun N, Wu Y, Nanba K, Sbiera S, Kircher S, Kunzke T, et al. High resolution tissue mass spectrometry imaging reveals a refined functional anatomy of the human adult adrenal gland. Endocrinology 2018.
17. Papathomas TG, Nose V. New and emerging biomarkers in endocrine pathology. Adv Anat Pathol 2019;26:198–209. [PubMed: 30730313]
18. Sun N, Kunzke T, Sbiera S, Kircher S, Feuchtinger A, Aichler M, et al. Prognostic relevance of steroid sulfation in adrenocortical carcinoma revealed by molecular phenotyping using high-resolution mass spectrometry imaging. Clin Chem 2019;65:1276–86. [PubMed: 31492715]
19. Murakami M, Rhayem Y, Kunzke T, Sun N, Feuchtinger A, Ludwig P, et al. In situ metabolomics of aldosterone-producing adenomas. JCI Insight 2019;4.
20. Murakami M, Sun N, Greunke C, Feuchtinger A, Kircher S, Deutschbein T, et al. Mass spectrometry imaging identifies metabolic patterns associated with malignant potential in pheochromocytoma and paraganglioma. Eur J Endocrinol 2021;185:179–91. [PubMed: 33983135]
21. Teuber JP, Nanba K, Turcu AF, Chen X, Zhao L, Else T, et al. Intratumoral steroid profiling of adrenal cortisol-producing adenomas by liquid chromatography- mass spectrometry. J Steroid Biochem Mol Biol 2021;212:105924. [PubMed: 34089832]
22. Meyer LS, Wang X, Susnik E, Burrello J, Burrello A, Castellano I, et al. Immunohistopathology and steroid profiles associated with biochemical outcomes after adrenalectomy for unilateral primary aldosteronism. Hypertension 2018;72:650–7. [PubMed: 30012870]
23. Gomez-Sanchez CE, Lewis M, Nanba K, Rainey WE, Kuppusamy M, Gomez-Sanchez EP. Development of monoclonal antibodies against the human 3beta-hydroxysteroid dehydrogenase/isomerase isozymes. Steroids 2017;127:56–61. [PubMed: 28863887]
24. Feuchtinger A, Stiehler T, Jutting U, Marjanovic G, Luber B, Langer R, Walch A. Image analysis of immunohistochemistry is superior to visual scoring as shown for patient outcome of esophageal adenocarcinoma. Histochem Cell Biol 2015;143:1–9. [PubMed: 25156293]
25. Edwards JL, Kennedy RT. Metabolomic analysis of eukaryotic tissue and prokaryotes using negative mode maldi time-of-flight mass spectrometry. Anal Chem 2005;77:2201–9. [PubMed: 15801754]
26. Shroff R, Muck A, Svatos A. Analysis of low molecular weight acids by negative mode matrix-assisted laser desorption/ionization time-of-flight mass spectrometry. Rapid Commun Mass Spectrom 2007;21:3295–300. [PubMed: 17880046]
27. Miura D, Fujimura Y, Tachibana H, Wariishi H. Highly sensitive matrix-assisted laser desorption ionization-mass spectrometry for high-throughput metabolic profiling. Anal Chem 2010;82:498–504. [PubMed: 20014780]
28. Miura D, Fujimura Y, Yamato M, Hyodo F, Utsumi H, Tachibana H, Wariishi H. Ultrahighly sensitive in situ metabolomic imaging for visualizing spatiotemporal metabolic behaviors. Anal Chem 2010;82:9789–96. [PubMed: 21043438]
29. Sun N, Ly A, Meding S, Witting M, Hauck SM, Ueffing M, et al. High-resolution metabolite imaging of light and dark treated retina using maldi-fticr mass spectrometry. Proteomics 2014;14:913–23. [PubMed: 24459044]
30. Wishart DS, Feunang YD, Marcu A, Guo AC, Liang K, Vazquez-Fresno R, et al. Hmdb 4.0: The human metabolome database for 2018. Nucleic Acids Res 2018;46:D608–D17. [PubMed: 29140435]

Author Manuscript Author Manuscript Author Manuscript Author Manuscript

31. Kanehisa M, Goto S. Kegg: Kyoto encyclopedia of genes and genomes. Nucleic Acids Res 2000;28:27–30. [PubMed: 10592173]
32. Chong J, Soufan O, Li C, Caraus I, Li S, Bourque G, et al. Metaboanalyst 4.0: Towards more transparent and integrative metabolomics analysis. Nucleic Acids Res 2018;46:W486–W94. [PubMed: 29762782]
33. Strohalm M, Kavan D, Novak P, Volny M, Havlicek V. Mmass 3: A cross-platform software environment for precise analysis of mass spectrometric data. Anal Chem 2010;82:4648–51. [PubMed: 20465224]
34. Buck A, Balluff B, Voss A, Langer R, Zitzelsberger H, Aichler M, Walch A. How suitable is matrix-assisted laser desorption/ionization-time-of-flight for metabolite imaging from clinical formalin-fixed and paraffin-embedded tissue samples in comparison to matrix-assisted laser desorption/ionization-fourier transform ion cyclotron resonance mass spectrometry? Anal Chem 2016;88:5281–9. [PubMed: 27065343]
35. Xia J, Wishart DS. Metpa: A web-based metabolomics tool for pathway analysis and visualization. Bioinformatics 2010;26:2342–4. [PubMed: 20628077]
36. Yang Y, Xiao M, Song Y, Tang Y, Luo T, Yang S, et al. H-score of 11beta-hydroxylase and aldosterone synthase in the histopathological diagnosis of adrenocortical tumors. Endocrine 2019;65:683–91. [PubMed: 31332713]
37. Rege J, Nakamura Y, Satoh F, Morimoto R, Kennedy MR, Layman LC, et al. Liquid chromatography-tandem mass spectrometry analysis of human adrenal vein 19-carbon steroids before and after acth stimulation. J Clin Endocrinol Metab 2013;98:1182–8. [PubMed: 23386646]
38. Arlt W, Lang K, Sitch AJ, Dietz AS, Rhayem Y, Bancos I, et al. Steroid metabolome analysis reveals prevalent glucocorticoid excess in primary aldosteronism. JCI Insight 2017;2.
39. Gao X, Yamazaki Y, Tezuka Y, Pieroni J, Ishii K, Atsumi N, et al. Intratumoral heterogeneity of the tumor cells based on in situ cortisol excess in cortisol-producing adenomas; approximately an association among morphometry, genotype and cellular senescence approximately. J Steroid Biochem Mol Biol 2020;204:105764. [PubMed: 33002589]
40. Calebiro D, Di Dalmazi G, Bathon K, Ronchi CL, Beuschlein F. Camp signaling in cortisol-producing adrenal adenoma. Eur J Endocrinol 2015;173:M99–106. [PubMed: 26139209]
41. Weigand I, Ronchi CL, Vanselow JT, Bathon K, Lenz K, Herterich S, et al. Pka calpha subunit mutation triggers caspase-dependent riibeta subunit degradation via ser(114) phosphorylation. Sci Adv 2021;7.
42. Beuschlein F, Fassnacht M, Assie G, Calebiro D, Stratakis CA, Osswald A, et al. Constitutive activation of pka catalytic subunit in adrenal cushing's syndrome. N Engl J Med 2014;370:1019–28. [PubMed: 24571724]
43. Rege J, Hoxie J, Liu CJ, Cash MN, Luther JM, Gellert L, et al. Targeted mutational analysis of cortisol-producing adenomas. J Clin Endocrinol Metab 2021.
44. Le Mestre J, Duparc C, Reznik Y, Bonnet-Serrano F, Touraine P, Chabre O, et al. Illicit upregulation of serotonin signaling pathway in adrenals of patients with high plasma or intra-adrenal acth levels. J Clin Endocrinol Metab 2019;104:4967–80. [PubMed: 31074783]
45. Kano K, Aoki J, Hla T. Lysophospholipid mediators in health and disease. Annu Rev Pathol 2021.
46. Pan CY, Wu AZ, Chen YT. Lysophospholipids regulate excitability and exocytosis in cultured bovine chromaffin cells. J Neurochem 2007;102:944–56. [PubMed: 17630986]
47. Koundouros N, Poulogiannis G. Reprogramming of fatty acid metabolism in cancer. Br J Cancer 2020;122:4–22. [PubMed: 31819192]
48. Wang W, Hao X, Han L, Yan Z, Shen WJ, Dong D, et al. Tissue-specific ablation of acsl4 results in disturbed steroidogenesis. Endocrinology 2019;160:2517–28. [PubMed: 31504388]

Author Manuscript Author Manuscript Author Manuscript Author Manuscript

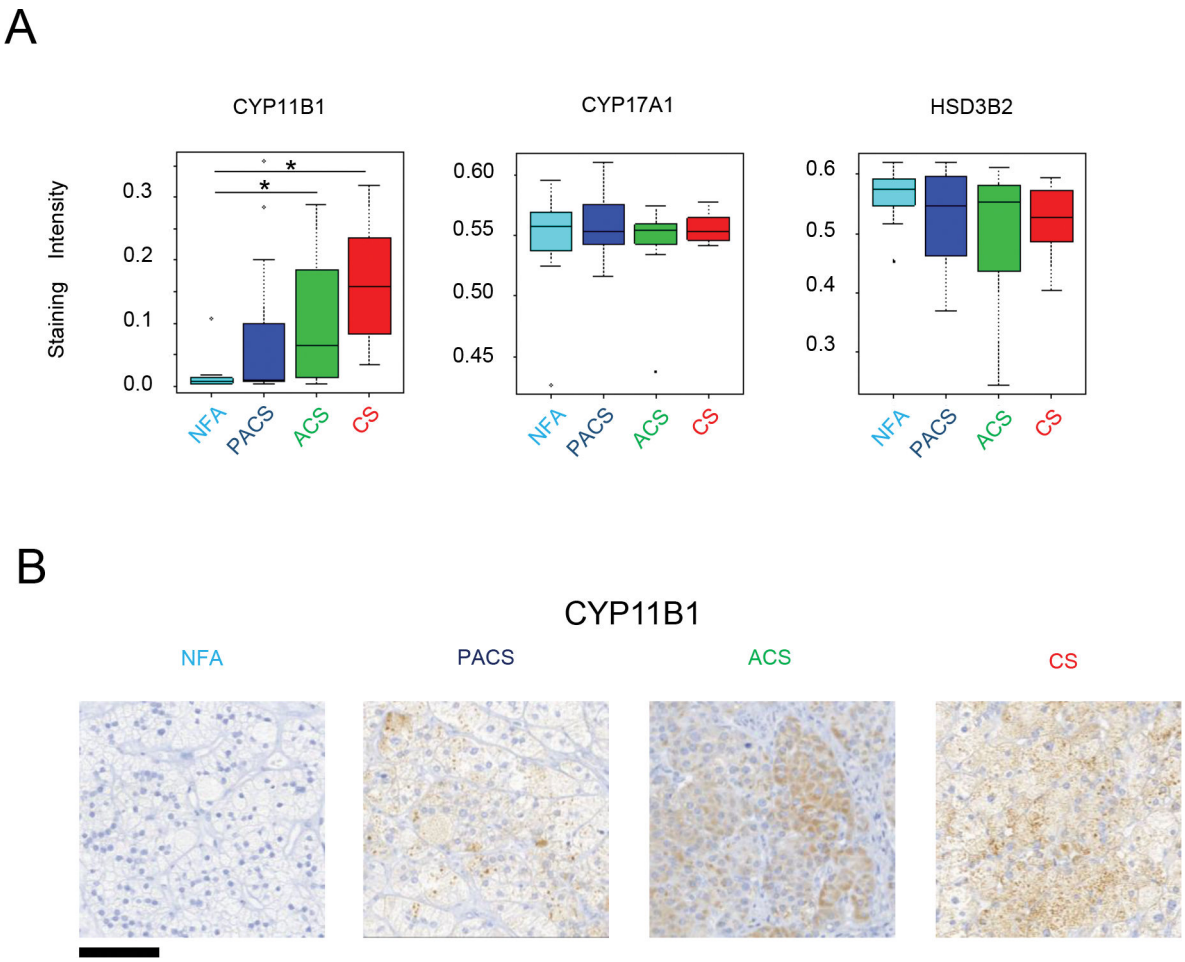

Figure 1:

Steroidogenic enzyme expression in 46 adrenal tumors.

Quantification of staining intensities for steroidogenic enzymes including CYP11B1, CYP17A1 and HSD3B2; correlations with cortisol-secretion phenotype ($P = 0.004$, 0.869 and 0.494, respectively, A). Representative images of immunohistochemistry of CYP11B1 were shown (B). Scale bar: 100 μm. *$P < 0.05$.

Author Manuscript Author Manuscript Author Manuscript Author Manuscript

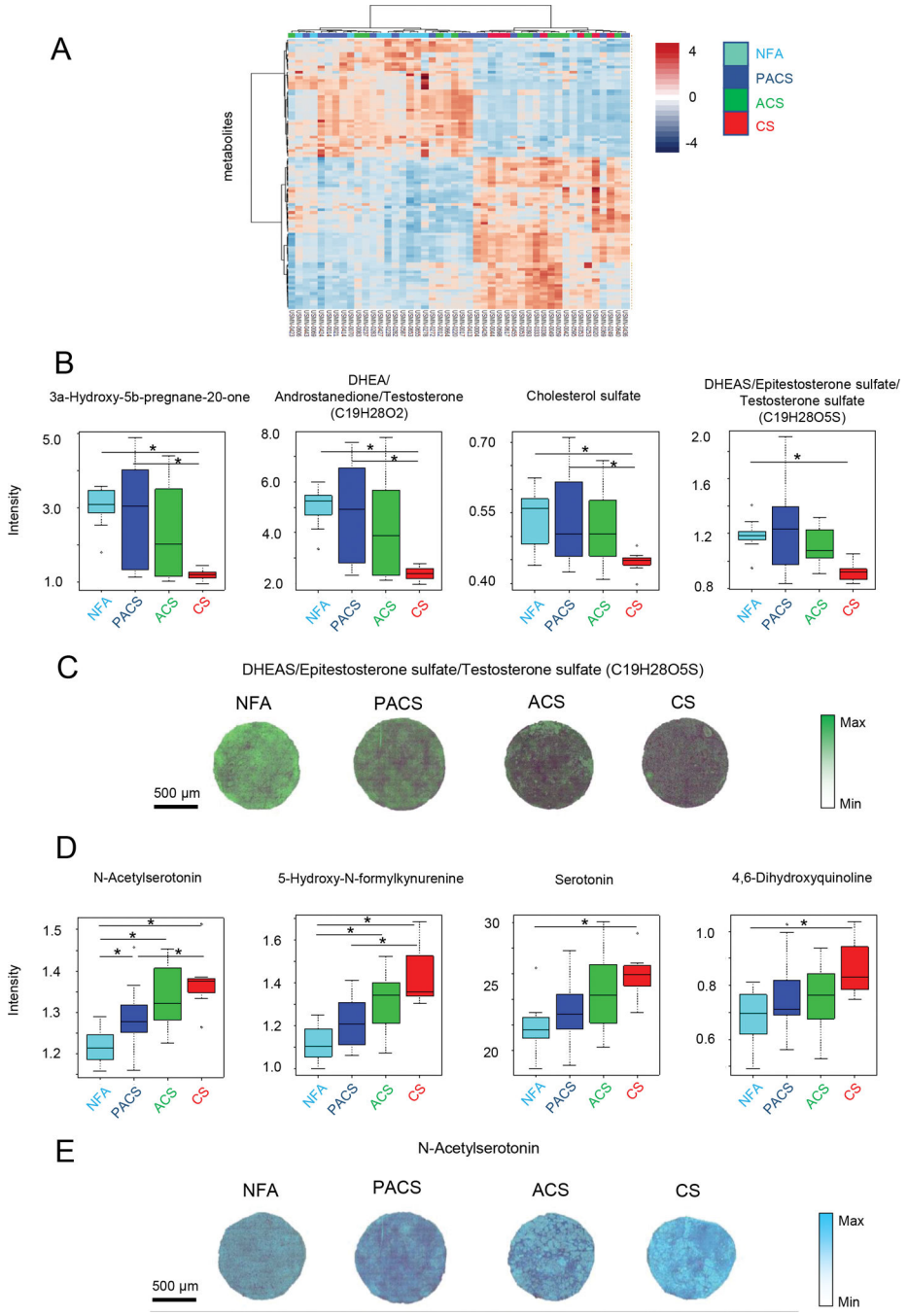

Figure 2:

Metabolome profiles and cortisol-secretion phenotype correlation.

Unsupervised hierarchical clustering analysis of metabolome profiles of 46 adrenal tumors with top 100 differential metabolites. (A). Intensities of steroid-related metabolites cholesterol sulfate, 3a-Hydroxy-5b-pregnane-20-one, C19H28O2 and C19H28O5S in cortisol-secretion phenotype were shown (B). Representative images of C19H28O5S were shown (C). C19H28O2 reflects the isobaric adrenal androgens derived from the classic androgen pathway: dehydroepiandrosterone (DHEA), androstanedione and testosterone,

Author Manuscript Author Manuscript Author Manuscript Author Manuscript

which could not be distinguished from each other in the applied technique. C19H28O5S reflects the classic adrenal androgen sulfates: dehydroepiandrosterone sulfate (DHEAS), epitestosterone sulfate and testosterone sulfate. Intensities of tryptophan metabolites N-acetylserotonin, 5-hydroxy-N-formylkynurenine, serotonin and 4,6-Dihydroxyquinoline in cortisol-secretion phenotype were shown (D). Representative images of N-acetylserotonin are shown (E). *P <0.05. Scale bars: 500 μm.

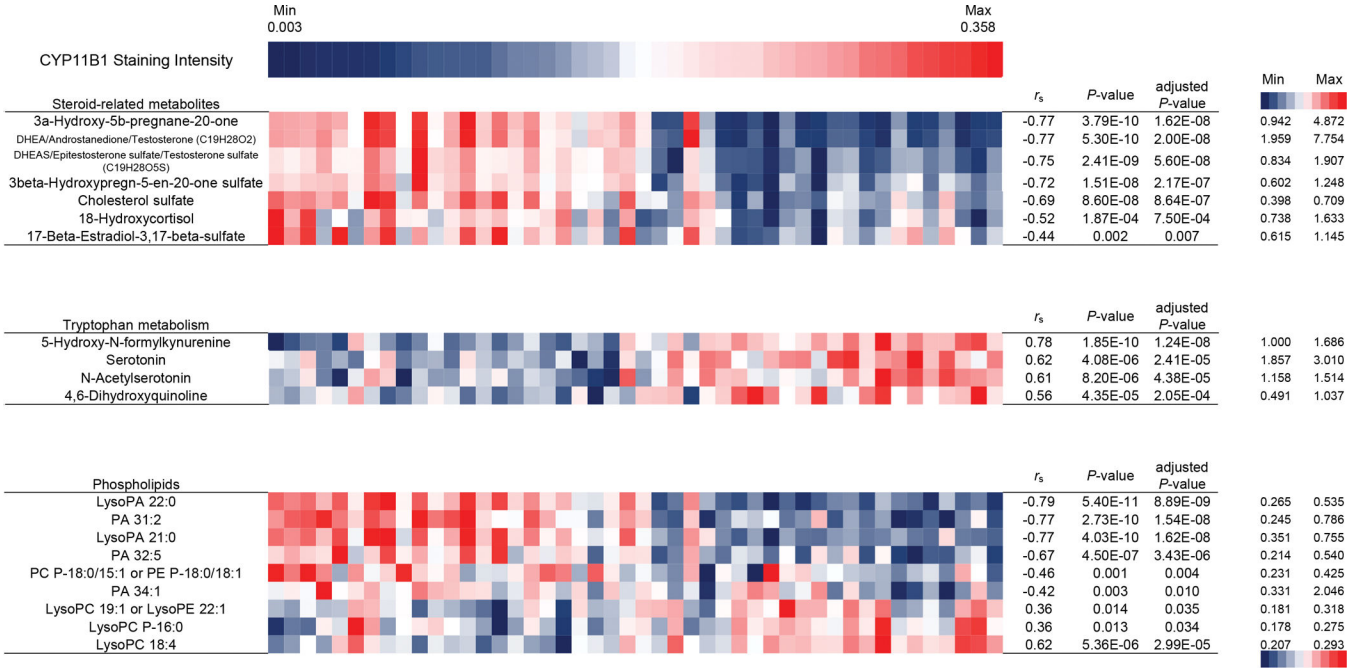

Figure 3:

Correlation of tumor metabolite content and steroidogenic enzyme expression. Heatmap visualizations of relationships between staining intensity of CYP11B1 and metabolites including steroid-related metabolites, tryptophan metabolites and phospholipids in linear scale. Spearman's rank correlation test was used for statistical analysis and Spearman's coefficient is denoted by r_s. *P*-value and adjusted *P*-value are shown. Minimum and maximum values of metabolites are shown next to the color bar.

Author Manuscript Author Manuscript Author Manuscript Author Manuscript

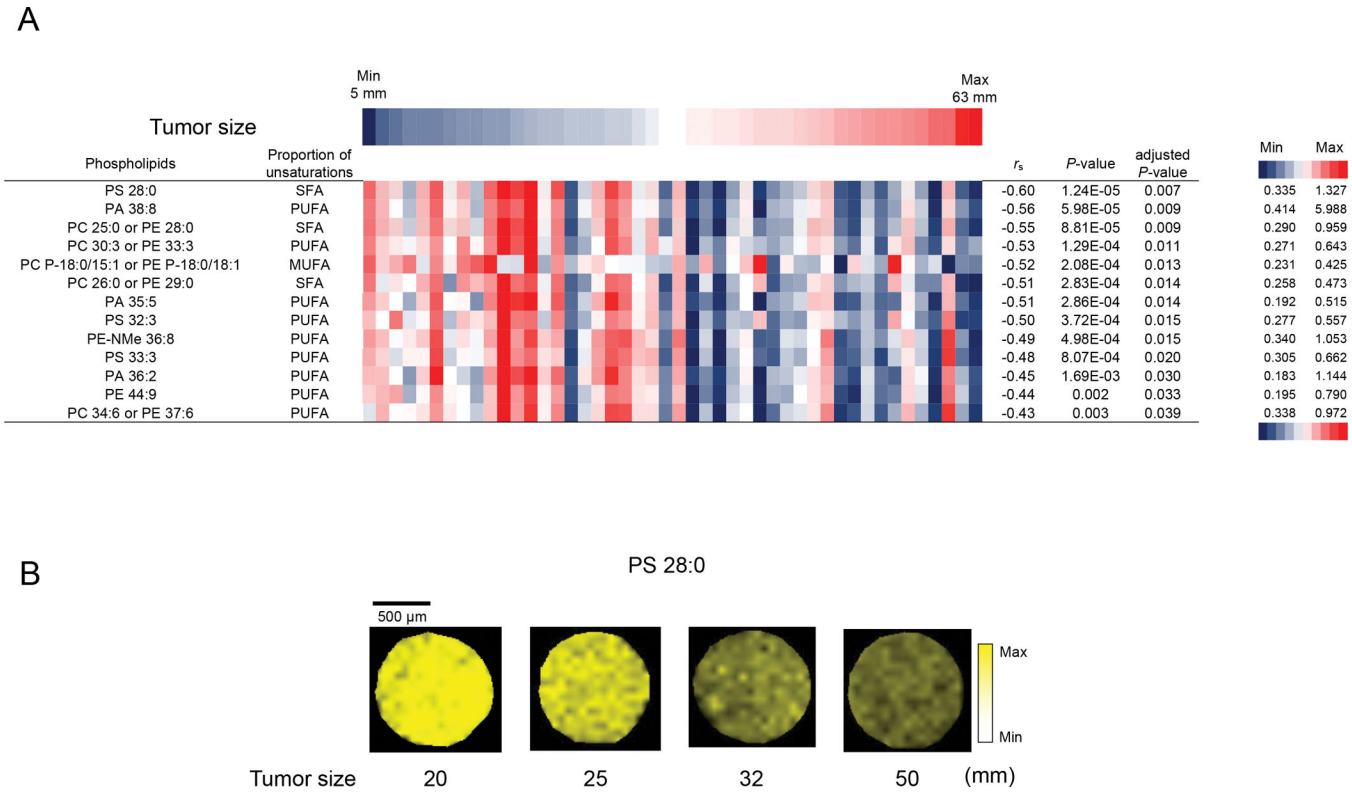

Figure 4:

Metabolome profiles and tumor size correlation.

Heatmap visualizations of relationships between tumor size and phospholipid contents in linear scale (A). Representative images of PS 28:0 were shown (B). Spearman's rank correlation test was used for statistical analysis and Spearman's coefficient is denoted by r_s. *P*-value and adjusted *P*-value are shown. Minimum and maximum values of metabolites are shown next to the color bar.

Author Manuscript Author Manuscript Author Manuscript Author Manuscript

Author Manuscript Author Manuscript Author Manuscript Author Manuscript

Table 1

A clinical characteristic of adrenal adenoma patients stratified by cortisol-producing ability. Data are presented as median (IQR).

		Sex						Cortisol			
		M	F	Age (years)	BMI (kg/m2)	Maximal tumor size (mm)	CT value (HU)	1mg DST (μg/dL)	UFC (μg/24h)	ACTH (pg/ml)	DHEAS (μg/ml)
Cortisol secretion ability		10	36	46	46	46	35	45 *	36	39	37
	46			51 (39 – 60)	30.7 (24.9 – 36.6)	32 (22 – 40)	7 (0 – 20)	3.7 (1.9 – 8.5)	20 (15 – 37)	7.5 (5.0 – 13.0)	0.307 (0.170 – 1.060)
NFA	11	2	9	43 (38 – 51)	32.8 (29.2 – 35.5)	19 (18 – 25)	9 (7 – 31)	1.1 (1.0 – 1.5)	15 (15 – 17)	12.0 (9.1 – 16.5)	0.795 (0.388 – 1.218)
PACS	16	5	11	54 (44 – 63)	30.5 (26.6 – 38.6)	36 (27 – 39)	3 (−9 – 8)	3.1a (2.4 – 3.7)	21 (17 – 32)	6.4 (5.0 – 12.7)	0.254 (0.170 –0.524)
ACS	12	2	10	44 (42 – 56)	29.0 (23.0 – 34.1)	33 (24 – 38)	21 (−1 – 32)	9.3a, b (6.8 – 12.5)	19 (16 – 27)	7.3 (5.9 – 9.8)	0.284 (0.150 – 1.278)
CS	7	1	6	59 (50 – 65)	26.1 (24.3 – 32.7)	42 (32 – 46)	6 (0 – 10)	14.5a, b (11.5 – 18.3)	36 (28 – 169)	5.0 (5.0 – 8.7)	0.572 (0.181– 1.490)
P-value				0.276	0.448	0.051	0.164	**1.61.E-08**	0.104	0.157	0.319

*One CS patient diagnosed with cortisol values after 8mg DST.

P-values of less than 0.05 were considered significant and shown in bold. $P<0.05$, compared to [a]NFA and [b]PACS.

BMI, body mass index; CT, computed tomography; DHEAS, dehydroepiandrosterone sulfate; DST, dexamethasone suppression test; UFC, urinary free cortisol concentration; NFA, non-functioning adenoma; PACS, possible autonomous cortisol secretion; ACS, autonomous cortisol secretion; CS, Cushing syndrome.